Last Interglacial–Glacial sequence of palaeosols and calcareous slope deposits at Verteuil (Charente, southwest France)

Jules Puyrigaud, Pascal Bertran, Brice Lebrun, Christelle Lahaye, Guillaume Guerin, Nicole Limondin-Lozouet

 ISSN 0267-8179. DOI: 10.1002/jqs.3538

JQS Journal of Quaternary Science QRA Quaternary Research Association

Last Interglacial–Glacial sequence of palaeosols and calcareous slope deposits at Verteuil (Charente, southwest France)

JULES PUYRIGAUD,[1] PASCAL BERTRAN,[1,2]* BRICE LEBRUN,[3] CHRISTELLE LAHAYE,[3] GUILLAUME GUERIN[4] and NICOLE LIMONDIN-LOZOUET[5]
[1]PACEA, UMR 5199 CNRS-Université de Bordeaux, allée Geoffroy-Saint-Hilaire, 33605 Pessac, France
[2]Inrap Nouvelle Aquitaine-Outre-Mer, 140 avenue du maréchal Leclerc, 33130 Bègles, France
[3]Archéosciences Bordeaux, UMR 6034, CNRS–Université Bordeaux Montaigne, Maison de l'archéologie, esplanade des Antilles, 33600 Pessac, France
[4]Géosciences Rennes, UMR 6118, CNRS–Université de Rennes 1, Campus Beaulieu, 35042 Rennes, France
[5]Laboratoire de Géographie Physique, UMR 8591 CNRS–Université Paris 1–UPEC, 2 rue Henri Dunant, 94320 Thiais, France

Received 3 February 2023; Revised 3 May 2023; Accepted 11 May 2023

ABSTRACT: The 12 m thick sequence of calcareous slope deposits and palaeosols exposed in a quarry at Verteuil (southwest France) has been studied and dated by optically stimulated luminescence. Emphasis was given to the identification and characterisation of palaeosols through geochemistry and micromorphology. The main clastic units, separated by major unconformities, were dated to MIS 6, MIS 5–4 and MIS 3–2. Stratified deposits ('grèzes litées'), consisting of alternating diamictic and matrix-free clastic beds and attributed to stacked stone-banked solifluction lobes, developed mainly after *ca.* 40 ka, i.e. during late MIS 3 and MIS 2. MIS 3 is recorded as a palaeosol complex including two humic A horizons overlying a chromic cambisol associated with burrows of ground squirrels, while MIS 5 corresponds to a reworked rubified chromic cambisol. Overall, this sequence shows similarities with the clastic deposits found in regional cave porches and rock shelters, strongly suggesting that anthropogenic activities did not significantly modify the climate-driven sedimentary and soil-forming processes at the Palaeolithic sites.

KEYWORDS: OSL dating; palaeosols; southwest France; stratified slope deposits; Weichselian

Introduction

Thick accumulations of limestone clasts at the foot of slopes are an important component of Quaternary formations in the Jurassic and Cretaceous terrains of the Aquitaine basin (southwest France). The clastic deposits formed in rock shelters and under the cave porches have given rise to extensive work because of abundant remains of Palaeolithic occupations. In these contexts, where rockfall and anthropogenic inputs contributed largely to sedimentation, deciphering the influence of climate remains difficult. In non-archaeological contexts, studies are scarcer and have mainly been dedicated to the analysis of sedimentary dynamics. The origin of stratified deposits ('grèzes litées') has been the focus of research for several decades (e.g. Guillien, 1951, 1954, 1964; Texier, 1986; Francou, 1990; Bertran et al., 1992, 1994). These studies have shown that the intrinsic factors of slope evolution related to the degradation of limestone outcrops over time by frost wedging and to the progressive growth of the talus, played a significant role in sedimentary dynamics and depositional facies. In Charente (Fig. 1), stratified deposits containing mostly small clasts (<2 cm) developed from compact limestone in small benches, mainly on Middle and Upper Jurassic terrain. They only occurred when the slope was previously regularised and when the fall of debris from a rock wall played only a marginal role (the deposits constitute a debris mantle, not a rockfall talus), while solifluction was active (Ozouf, 1983; Bertran et al., 1992). Stratified deposits are prevalent on east-facing slopes, presumably because they were most favourable to freeze–thaw cycles that ensured size reduction (Aubry and Lautridou, 1974; Lautridou and Leneuf, 1974) and efficient downslope transport of clasts. As these studies preceded the widespread use of luminescence dating methods and as organic remains that can be dated by radiocarbon were lacking, the evolution of slope dynamics in relation to Pleistocene climatic variations remained poorly documented.

This work aims to analyse the calcareous slope deposits exposed in a quarry at Verteuil (Charente), which shows a succession of clastic deposits and palaeosols over a thickness of nearly 12 m. It is located near the quarry previously studied by Bertran et al. (1992, 1994), where the stratified deposits have been described in detail. Emphasis has been given to the identification and characterisation of palaeosols through geochemistry and micromorphology, as well as to the establishment of a precise chronological framework based on optically stimulated luminescence (OSL) dating. The deposits, although discontinuous, cover a long time interval from the Penultimate Glacial (Saalian) to the Holocene, and for the first time allow a detailed chronostratigraphy to be established for this type of deposit in southwest France.

Material and methods

Geomorphological setting

The quarry (x = 0.229051°E, y = 45.974193°N) is located in the Charente valley a few hundred metres south of the village

*Correspondence: P. Bertran, as above.
E-mail: pascal.bertran@inrap.fr

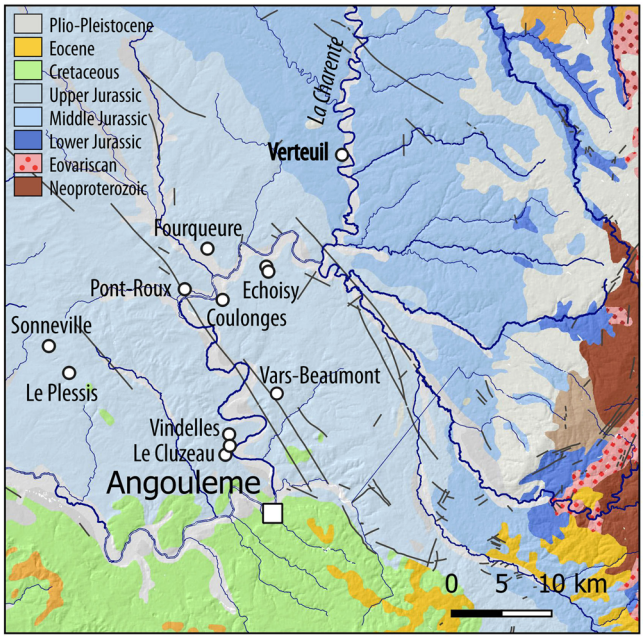

Figure 1. Extract from the 1:1,000,000 digital geological map of France (https://infoterre.brgm.fr/) showing the location of the studied section and other sections of stratified slope deposits (white circles) mentioned in the literature. [Color figure can be viewed at wileyonlinelibrary.com]

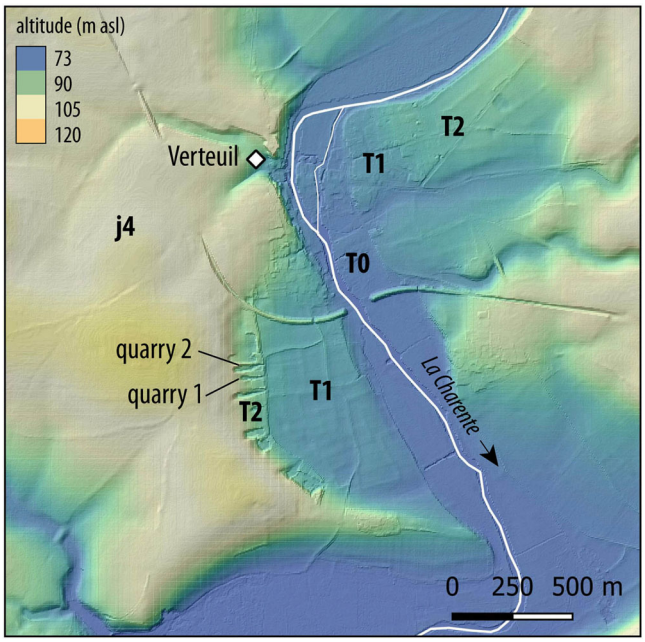

Figure 2. Topographic map of the studied area (RGEALTI 5 m, Institut Géographique National) and location of the quarry studied by Bertran et al. (1992, 1994) ('quarry 1') and of the new quarry ('quarry 2'). T0: alluvial plain; T1, T2: alluvial terraces; j4: Jurassic limestone. [Color figure can be viewed at wileyonlinelibrary.com]

of Verteuil (Fig. 1). The deposits developed at the foot of a long east-facing slope of Callovian (Middle Jurassic) limestone (Fig. 2). It is a light grey to yellowish micritic limestone, with small marly benches, especially at the top (Cariou and Gabilly, 1973). The limestone outcrops largely upslope, where the gradient is low (2–5°). Further downslope, the gradient reaches up to 12–13° and then decreases steadily to become negligible in the most distal part. The topographic profile made from the IGN 5 m LiDAR survey (RGEALTI 5 m) shows that the distal flat area corresponds to a terrace, probably of alluvial origin, dominating the present floodplain by about 11 m (Fig. 3). This terrace, here labelled T2, developed in a concave meander on the right bank of the river. The slope deposits thus form a prism at the foot of the slope and overlie the alluvial formations.

Methods

Fieldwork

The stratigraphy was studied in detail along the southern wall of the quarry. Because of the dip of the layers, two sections were analysed to cover the entire sequence: one downslope for the upper units (section A), and an upslope for the lower units (section B) (Fig. 4). Despite the use of a telescopic ladder, the top of the section could not be reached. Therefore, a complementary section (log C) was analysed in a nearby, more easily accessible quarry, 110 m to the south. This quarry, now largely filled with trash, was previously studied by Bertran et al. (1992, 1994). The sections were manually cleaned and then described and sampled every 10–20 cm in the matrix-rich layers. The apparent dip of the layers was measured with an inclinometer.

Sedimentological and geochemical analyses

Nine undisturbed samples were collected for thin-section preparation, after applying a mixture of water and sodium silicate (consolidant) with a sprayer to the blocks of sediment. The samples were dried in an oven and then impregnated under vacuum with a polyester resin. The thin sections were studied with a Leica 2500P polarising microscope and described according to Bullock et al. (1985).

The volumetric magnetic susceptibility was measured in the field approximately every 10 cm using a Bartington MS2 instrument equipped with an MS-2F probe, representing 80 measurement points. Particle-size analysis was performed with a HORIBA LA-950 microgranulometer on the fraction finer than 2 mm from 47 samples after sieving with water, removal of organic matter (H_2O_2), dispersion with sodium hexametaphosphate (5 g/L) and treatment in an ultrasonic tank (60 s). Colorimetry was performed in the laboratory on the dry fine-grained fraction (<100 µm) of the same samples using an AvaSpec2048 spectrometer for wavelengths from 200 to 1100 nm. The Red Index was calculated using the formula of Barron and Torrent (1986) and Viscarra Rossel et al. (2006) to quantify the intensity of sediment rubefaction.

Total organic carbon (TOC) content was measured by infrared spectrometry on the fraction finer than 100 µm from 25 samples using a Leco CS-125 analyser at the EPOC laboratory (University of Bordeaux-CNRS) after decalcification (2N HCl). The geochemical study was performed at the PACEA laboratory by energy dispersive X-ray fluorescence spectrometry (ED-XRF) using a Bruker Tracer 5i on the fine-grained fraction (<100 µm) from 47 samples. This fraction was ground and then compacted with 0.03% wax ($C_{38}H_{76}N_2O_2$) to form 300 mg pellets. Two measurements were taken under vacuum for all samples, one at 15 kV and 100 µA for 300 s without filter to measure light elements and the other at 50 kV and 35 µA for 120 s with a Cu75, Ti25, Al200 filter for heavy elements. Since the sediments originate primarily from the fragmentation of limestone, the concentrations of the various elements are highly dependent on Ca variations. To eliminate the Ca dilution effect and to better evaluate the fluctuations of the elements hosted by silicate minerals, the Si/Al, Zr/Al and Rb/K ratios were calculated. Si/Al reflects the relative abundance of quartz and aluminous silicates, while Zr/Al is an indicator of aeolian silt inputs, as loess typically shows significant Zr enrichment relative to sources (Gallet et al., 1998; Bosq et al., 2020).

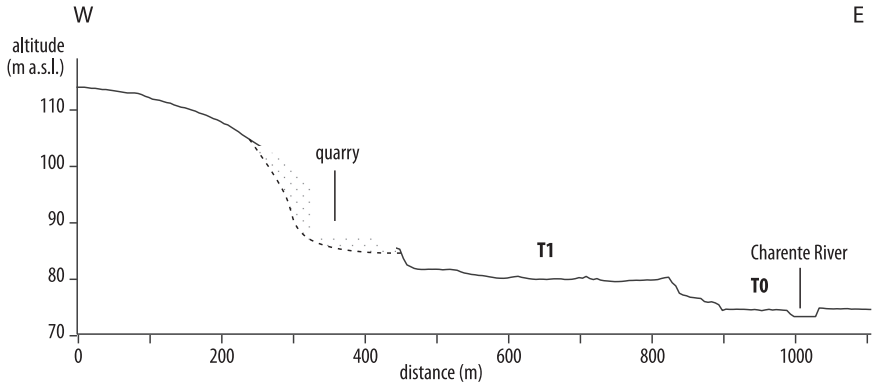

Figure 3. Topographic profile extracted from the 5 m DEM (RGEALTI) and location of the quarry. The slope deposits correspond to the dotted area.

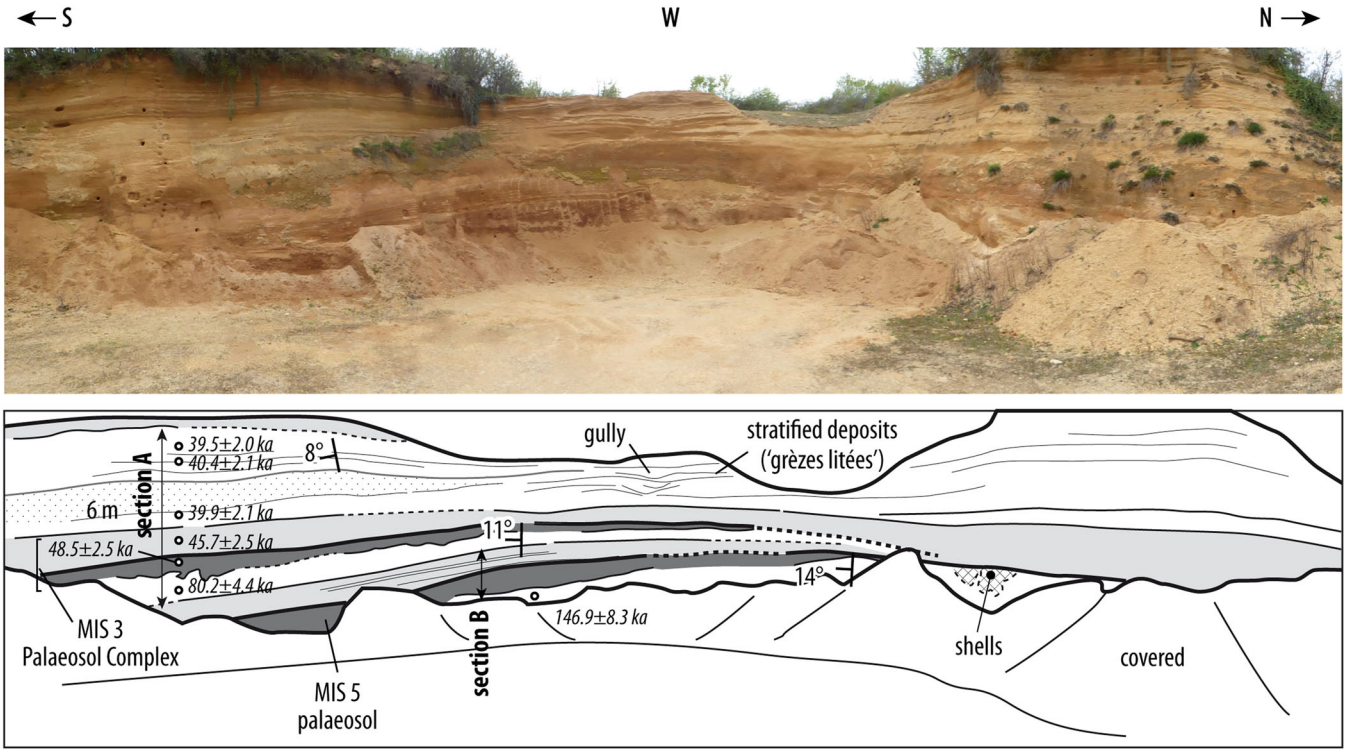

Figure 4. General photograph of the quarry (looking west) and interpretation. [Color figure can be viewed at wileyonlinelibrary.com]

Rb/K is an index of chemical alteration of K-bearing minerals (Nesbitt et al., 1980; Sheldon and Tabor, 2009; Buggle et al., 2011).

Malacology

The search for molluscan shells and earthworm calcite granules by sieving proved disappointing, mainly because of the difficulty of identifying them in a carbonate-rich heterogeneous sediment. Only one locus yielded shells, which were visible to the naked eye in the field. The shells were collected individually from the section.

Luminescence dating

Seven samples distributed over the entire sequence were taken for OSL dating at the Archéosciences Bordeaux laboratory using metal tubes driven into the sections. Field gamma-ray spectrometry measurements (LaBr, INSPECTOR 1000) were performed at the locations of the collected samples. External dose rates were thus determined for each sample, thanks to the *in situ* gamma-spectrometry measurements, using the 'Gamma' R-package (Lebrun et al., 2020) and the threshold technique (Miallier et al., 2009; Guérin and Mercier, 2011). The K–U–Th content of each sample was measured by high-purity low background gamma-spectrometry (Guibert and Schvoerer, 1991) in the laboratory, and used to determine the alpha and beta dose rates using conversion factors from Guérin et al. (2011), grain-size attenuation factors from Guérin et al. (2012a) and moisture correction factors from Zimmerman (1971) and Aitken and Xie (1990).

For equivalent dose measurements, samples were prepared according to a standard protocol, including: (1) sieving with water to isolate the grain-size fraction of interest; (2) removal of carbonates using 10% HCl for 1 h; (3) removal of organic compounds by H_2O_2 etching for 24 h; and (4) cleaning of the surface of the grains and removal of feldspars via a solution of 30% H_2SiF_6 and 68% HNO_3 at a ratio of 10/1 mL. The 20–40 µm quartz fraction was selected. Luminescence measurements were performed using a Lexsyg Smart system (Freiberg Instruments, Richter et al., 2015), equipped with a $^{90}Sr/^{90}Y$ calibrated beta source, delivering a dose of 0.162 ± 0.006 Gy/s to the sample at the time of measurements. A multigrain single-aliquot regenerative dose protocol (SAR) was adopted (Murray and Wintle, 2000, 2003; Wintle and Murray, 2006). Dose recovery tests were performed, as well as a preheat

plateau test; the best measurement conditions were thus determined. Pseudo-linearly modulated OSL tests (Bulur, 2000; Bos and Wallinga, 2012) showed that the quartz OSL signal is dominated by the fast OSL component in all cases. For each sample, a minimum of 14 aliquots was measured.

Results

Stratigraphy

The synthesis of the stratigraphy exposed at the three sections is shown in Fig. 5. Different facies have been identified mainly based on stratification, microstructure and colour. They include:

(1) Stratified units, comprising alternating yellow-brown to red-brown dominantly clast-supported diamictic beds, and openwork clastic beds (units C2, A2 and A10–B1) (Fig. 6A). The thickness of the beds ranges from 5 to 30 cm. The diamictic beds extend over tens of metres in longitudinal section. They sometimes show small recumbent folds at the base (Fig. 6B). Matrix-poor levels often show either normal or reverse grading (particle size decreases/increases from the base to the top), or grading with double polarity (a combination of normal grading at the top and reverse grading in the basal part) (Fig. 6C). When it can be determined, the orientation of the clast elongation axis is parallel to the slope. Strong clast imbrication is also often visible. At the microscopic scale, features related to segregation ice lenses and eluviation (silty caps on clasts, washed sand-grain accumulation, platy and vesicular microstructure, e.g. Van Vliet-Lanoë, 2010) (Fig. 6D, E) are abundant in matrix-rich beds.

(2) Massive or crudely stratified diamictic units 0.3–1 m thick, dominantly clast supported, composed of centimetre-sized clasts and a yellow-brown (10YR, units A1, A4, B3) to red-brown (7.5YR, unit A9) silty matrix (Fig. 7A). As in the

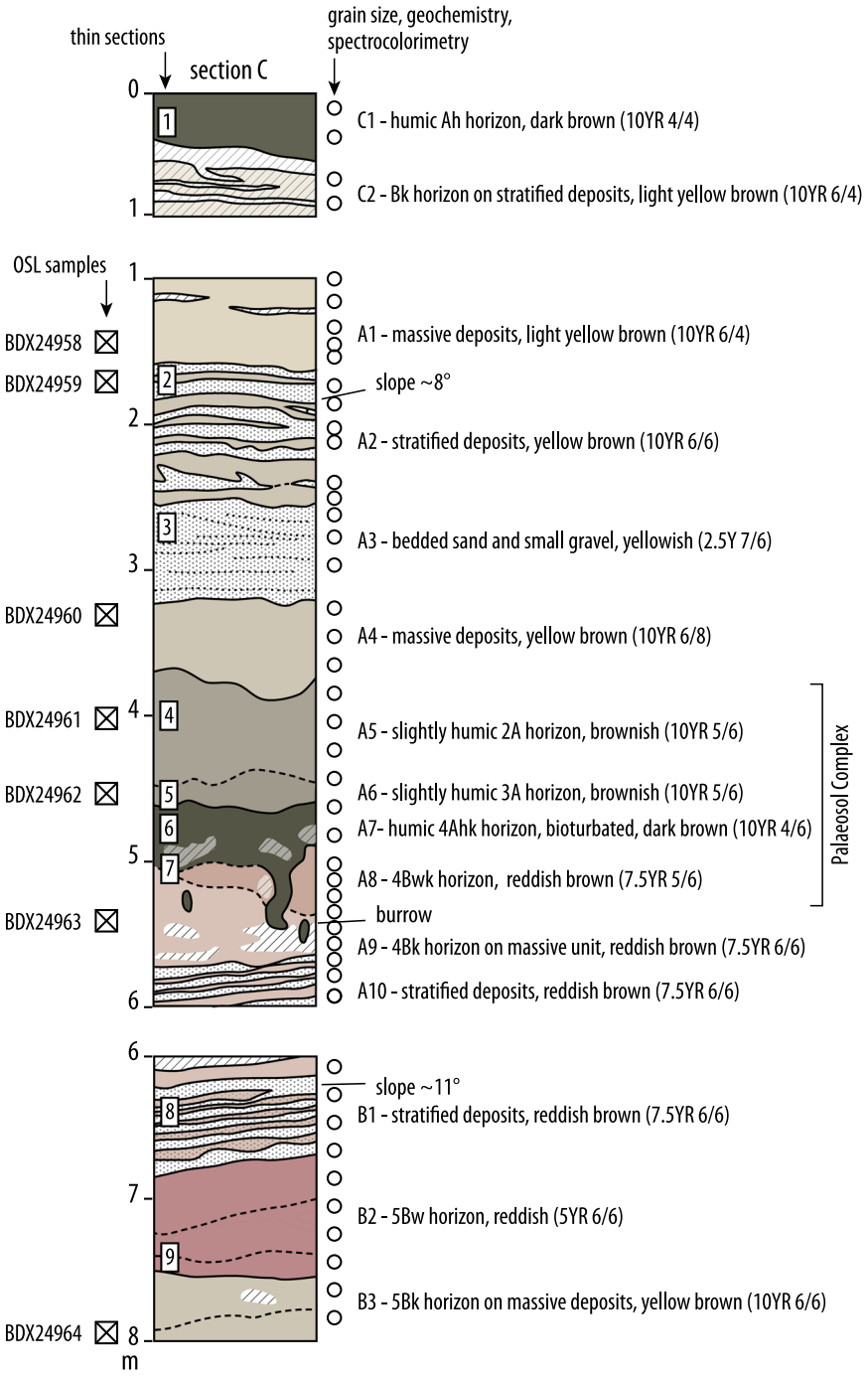

Figure 5. Schematic section and location of the analysed samples. [Color figure can be viewed at wileyonlinelibrary.com]

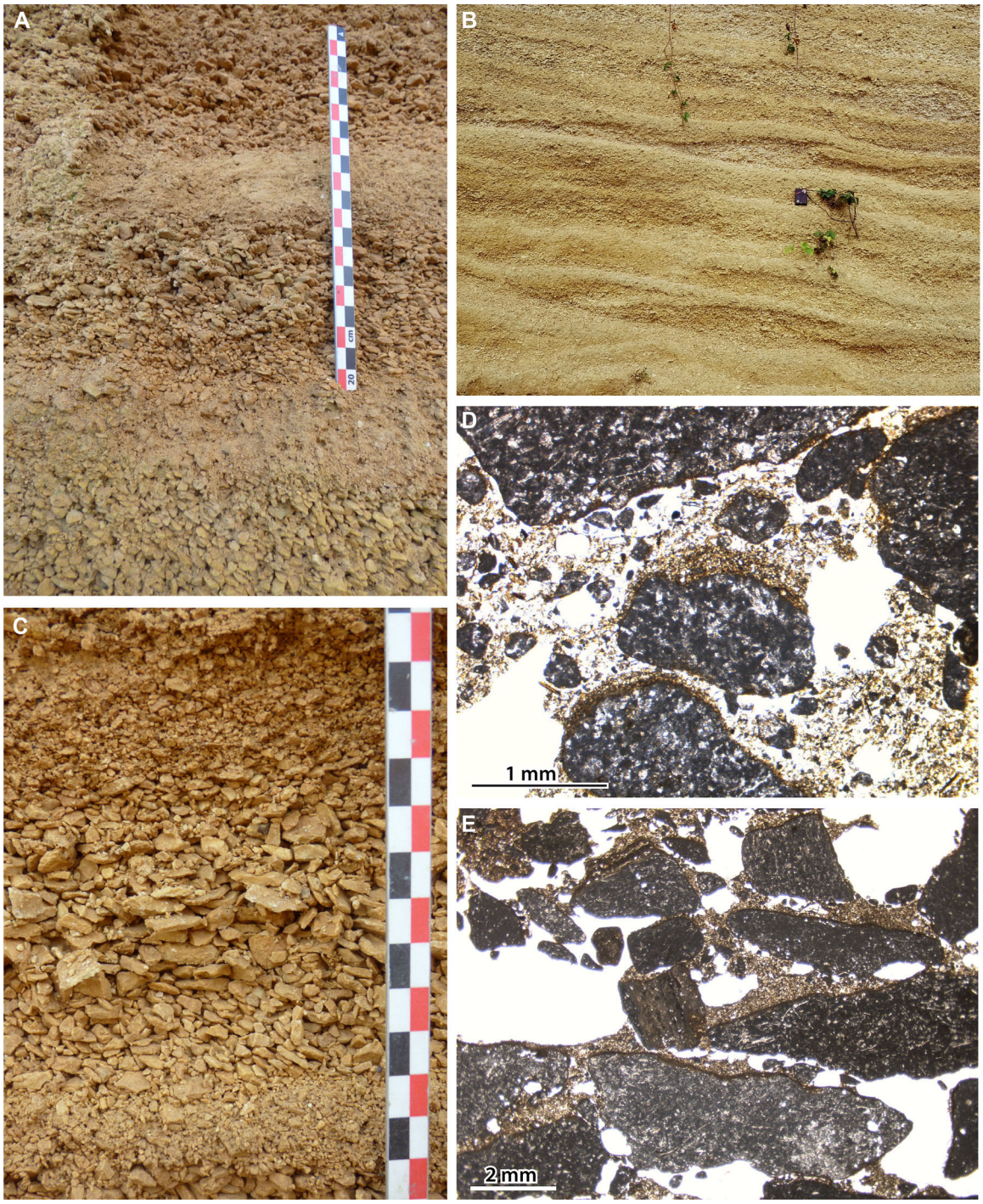

Figure 6. View of stratified facies. A – unit A2; B – recumbent folds at the base of matrix-rich beds, unit A2 (quarry 1); C – grading with double polarity, unit B1; D – washed sandy matrix and silty caps on clasts, unit A2; E – silty caps and vesicular porosity, unit B1. [Color figure can be viewed at wileyonlinelibrary.com]

stratified facies, the clasts have a preferential orientation parallel to the slope and locally show strong imbrication.

(3) Sorted calcareous sand and fine gravel with dominant sub-horizontal bedding, forming large nested lenses between 2.7 and 3.2 m depth (unit A3) (Fig. 7B). Bedding is locally indistinct, with bed boundaries often blurred. The finer-grained beds show a platy structure at the microscopic scale (Fig. 7D).

(4) Matrix-supported partly humic (A) horizons, stained brown to dark brown by organic matter (units C1, A5, A6 and A7) (Fig. 8A, B). Under the microscope, abundant bioturbation and faecal aggregates are visible (Fig. 8C, E), as well as secondary carbonate precipitation as root cell pseudomorphs (Fig. 8F) and accumulations of calcite needles. Carbonate precipitations form a Bk horizon below units C1 and A7. In the superficial Ah horizon and to a lesser degree in unit A6, fissure porosity (polyhedral structure) is well developed, whereas cryogenic porosity (platy to granular structure) dominates in unit A7 (Fig. 8D). Burrows (crotovinas) ranging from 6 to 14.5 cm in diameter (mean 9.5 cm) develop beneath unit A7. By comparison with data published by Ponomarenko and Ponomarenko (2019), the size of the burrows makes it possible to attribute them to ground squirrels (*Spermophilus* sp.) and potentially, for the smallest, to the European hamster (*Cricetus cricetus*), both species whose presence in France during the Last Glacial has been documented (Royer et al., 2016).

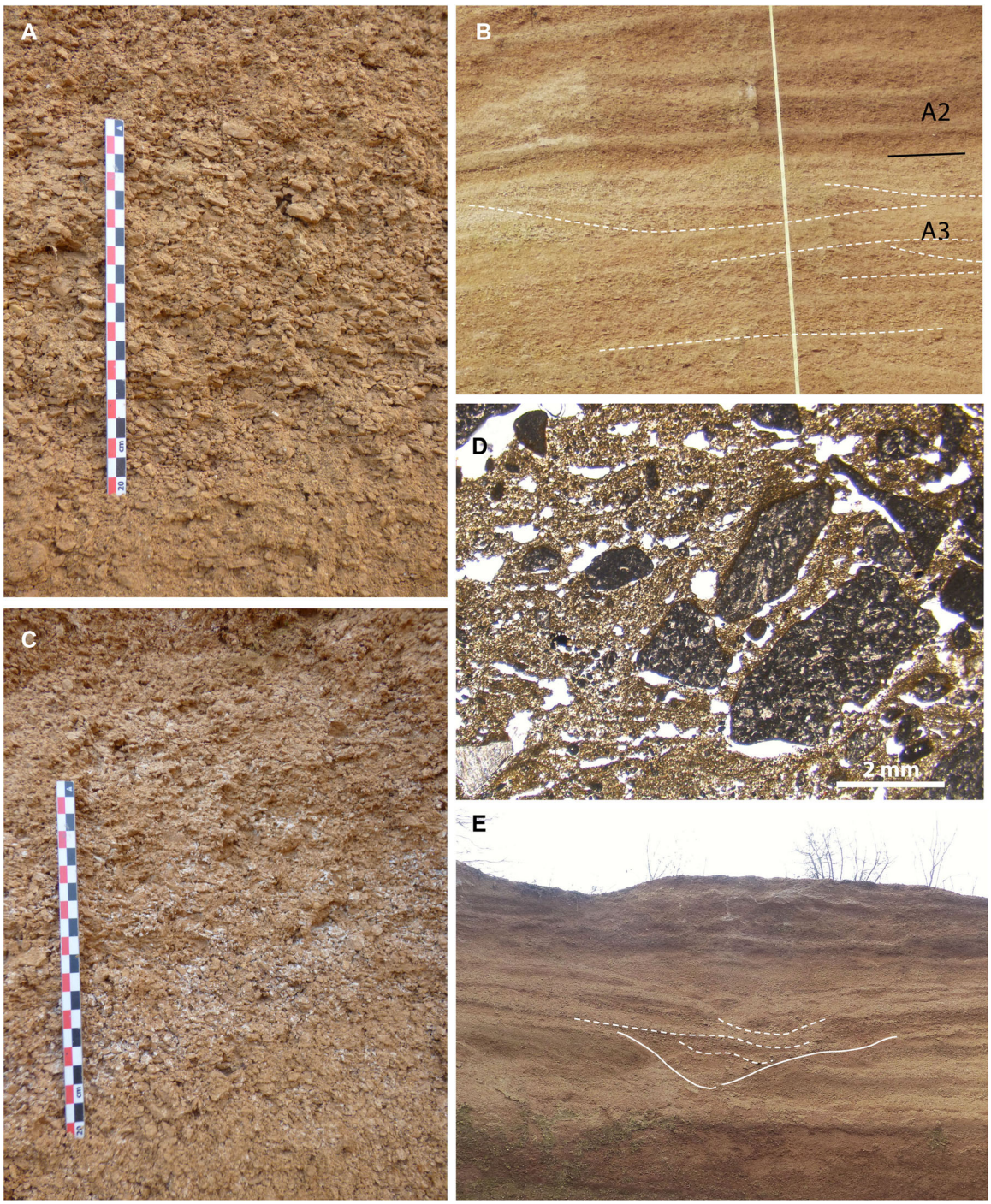

Figure 7. View of various facies. A–massive deposits, unit A4, the scale is 20 cm; B–massive deposits, unit A9; C–sand and fine gravel (unit A3) overlaid by stratified deposits (unit A2), the section is 1.5 m high; D–sandy-silt bed with platy structure, unit A3; E– view of the western wall of the quarry (section perpendicular to the slope) showing a gully; the section is approximately 4 m high. [Color figure can be viewed at wileyonlinelibrary.com]

(5) Reddish brown to reddish cambic horizons (Bw) (units A8, 7.5YR and B2, 5YR) (Figs 8A, 9A). Unit A9 is characterised at the microscopic scale by incomplete matrix decalcification and abundant features of secondary carbonate accumulation, primarily as calcite needle coatings in the voids. The superposition of three A horizons (units A6, A7, A8) and one Bw horizon (unit A9) in the middle part of the sequence is referred to here as a 'palaeosol complex'. Unit B2, with an almost totally decalcified rubified matrix, shows some biological features (galleries clogged with faecal aggregates, root cell pseudomorphs) (Fig. 9C) intersecting features of cryogenic origin (thin clay caps around the clasts, rounded clay aggregates, poorly developed platy structure) (Fig. 9D, E). Numerous small, sharp-contoured Fe-Mn concretions are present.

Magnetic susceptibility, spectrocolorimetry, TOC

Magnetic susceptibility remains low throughout the sequence (Fig. 10), with values lower than 10×10^{-6} SI except in the A horizons (unit C1 and A7, 30 to 50×10^{-6} SI) and, more markedly, in the 5Bw horizon (unit B2, 80×10^{-6} SI). Magnetic susceptibility fluctuates in relation to the abundance of magnetic mineral particles in the sediments. Since limestone yields extremely low values, these particles are mostly iron oxides formed in the soil by bacterial activity and redox processes associated with

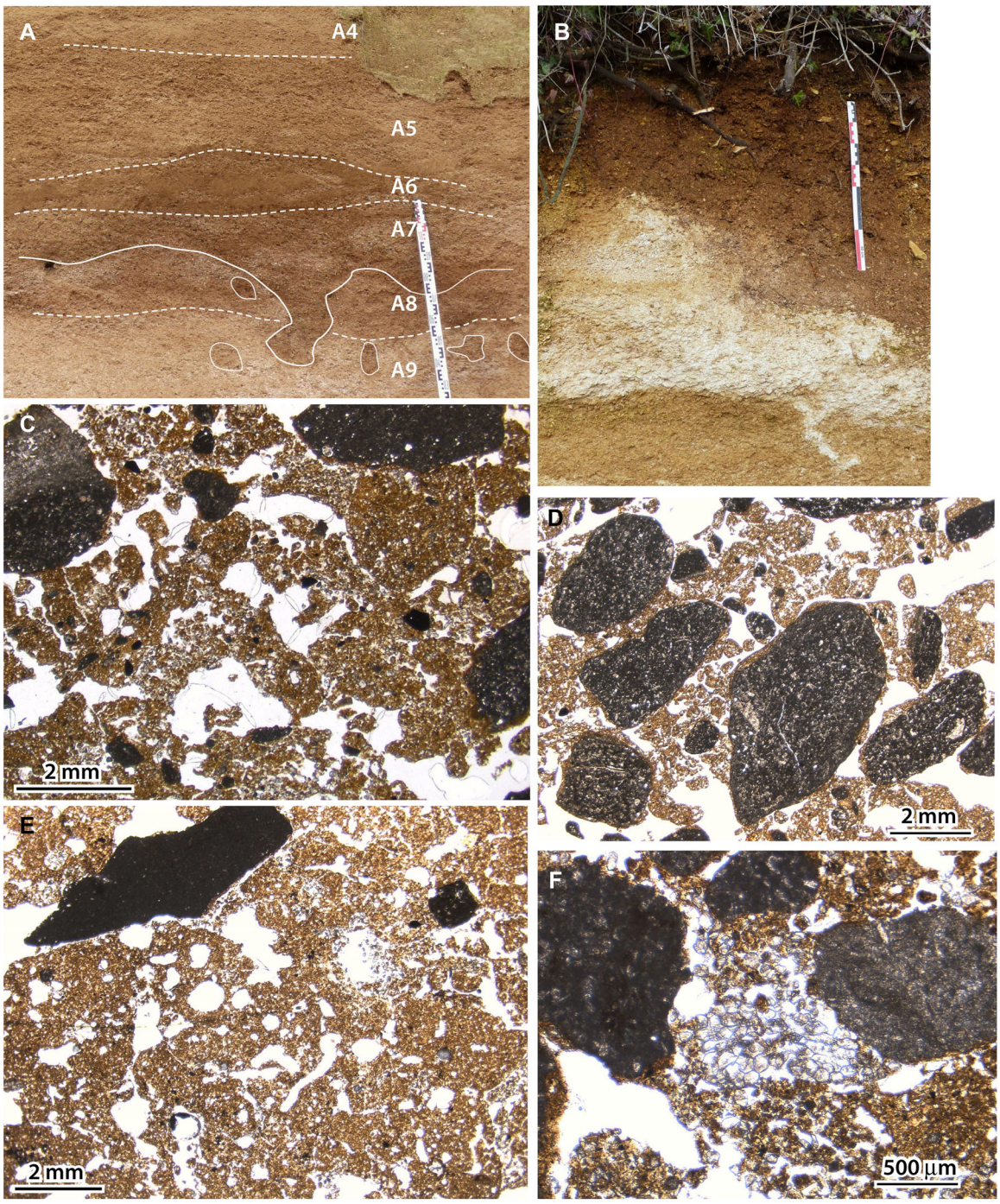

Figure 8. View of the humic horizons. A – MIS 3 palaeosol complex; scale is 80 cm; B – Holocene soil (quarry 1); scale is 50 cm; C – biological porosity and faecal aggregates, horizon 2A (unit A5); D -silty caps on clasts and rounded cryogenic aggregates, horizon 4Ak (unit A7); E- biological porosity, horizon 3A (unit A6); F – calcitic root cell pseudomorphs, horizon 2A (unit 5). [Color figure can be viewed at wileyonlinelibrary.com]

waterlogging (Mullins, 1977; Maher and Thompson, 1991; Ellwood et al., 2004). Oxide production either occurred *in situ* on the slope or on the plateau, with magnetic particles subsequently mixed with limestone debris by slope dynamics. Here, the highest values are associated with soil horizons and thus suggest dominant *in situ* production. These horizons are also characterised by high values on the Red Index (rubefaction) and TOC. TOC reaches 2.5% in the Holocene Ah horizon, while it does not exceed 0.5 to 0.7% in the buried A horizons (units A5, A6 and A7) due to partial mineralisation of organic molecules over time. The 5Bw horizon (Unit B2) is also characterised by TOC values only slightly higher (~0.3%) than those of clastic levels. The lowest values are from stratified deposits (0.1–0.2%).

Grain size

The facies identified show variations in their grain-size composition (Fig. 11). The stratified deposits contain little clay (7–17%) and the samples are distributed along a line parallel to the sand–silt axis in the triangular texture diagram. Examination of the grain size curves reveals a peak in fine silts between 14 and 20 µm, mostly represented in the stratified deposits (Fig. 12). In contrast, the soil horizons have low sand content (<20%) and are enriched in clay (30–40%). Samples of massive deposits have a more scattered composition, intermediate between those of stratified deposits and soil horizons.

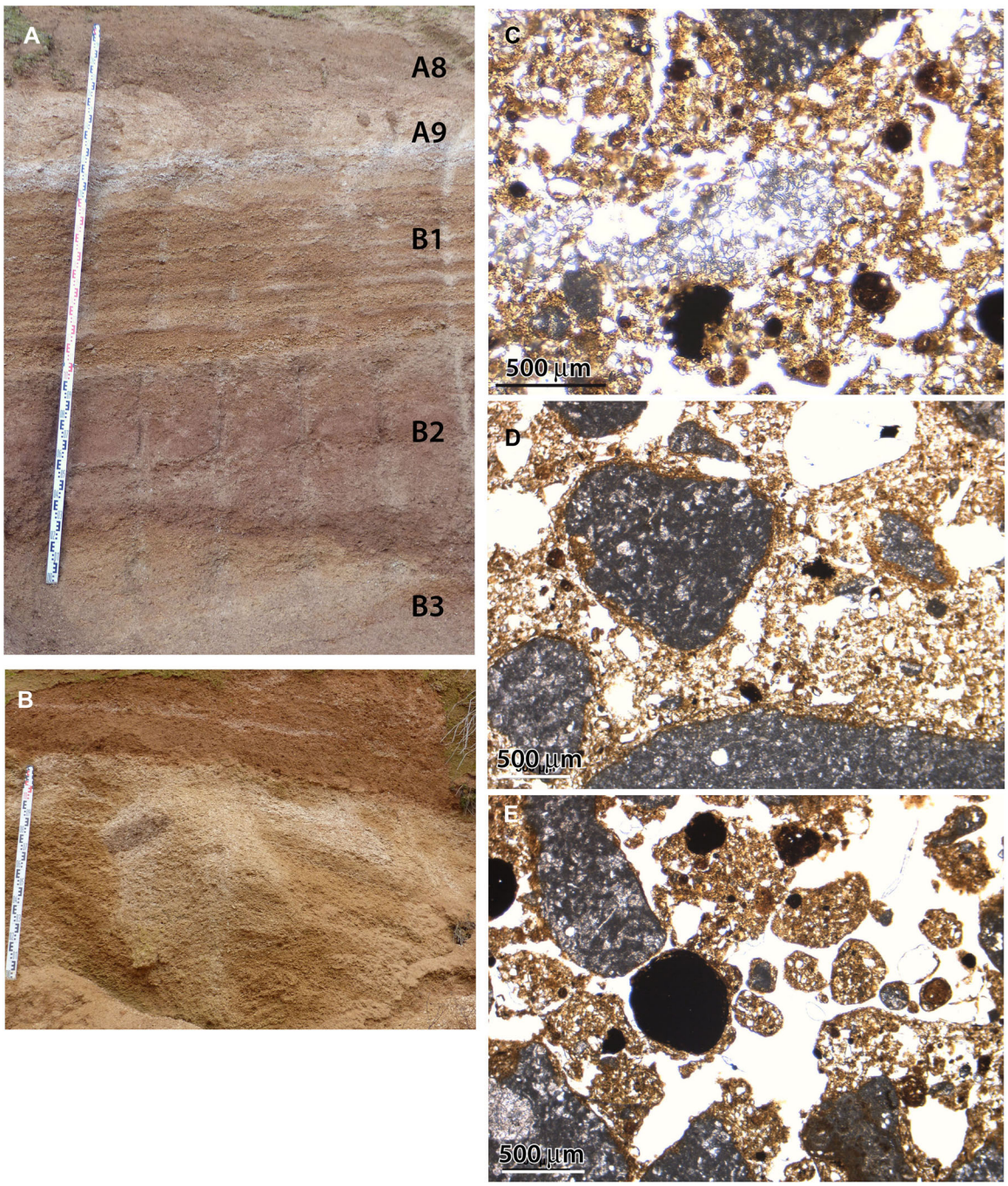

Figure 9. View of horizon 5Bw (unit B2). A–general view, scale is 3 m; B–loose area rich in secondary carbonates in unit B3, which yielded *Cepaea* shells, scale is 1 m; C–calcitic root cell pseudomorphs; D–clay caps around clasts; E–rounded cryogenic aggregates and Fe-Mn concretions. [Color figure can be viewed at wileyonlinelibrary.com]

Geochemistry

The Ca content is relatively constant in the massive and stratified deposits and is around 30% (Fig. 10). Ca reaches the lowest values in the A and Bw horizons (around 10%), which indicates partial decalcification. Concomitantly, secondary accumulation of carbonates is observed under these horizons (Bk). The partially decalcified levels also have larger than average Rb/K values (6 to 8 × 10^5, mean of all samples = 5.2 × 10^5), suggesting alteration of K-bearing silicates (micas/illite, K-feldspars).

In the stratified deposits (Unit A2, B1), the geochemical composition shows high values for Si/Al (5.1 to 6.0, mean of all samples = 4.1) and Zr/Al (0.054 to 0.064, mean of all samples = 0.046) ratios. The first ratio indicates an enrichment in silicate minerals, while the second shows zircon-rich inputs. Altogether, this suggests inputs of silicate-rich aeolian dust.

Malacology

The six shells collected came from an area rich in secondary carbonates located below unit B2 (5Bw) and interpreted as the remnant of an ancient root system or a windthrow (Fig. 9B). They are recrystallisations of internal moulds. Five belong to the genus *Cepaea* and one is identified as the taxon *Hygromia limbata*. In the current fauna of France, the genus *Cepaea* is mainly represented by two species, *C. hortensis* and *C. nemoralis*, that can coexist in a variable range of well-vegetated biotopes from tall grass to open woods, and both species are widely distributed

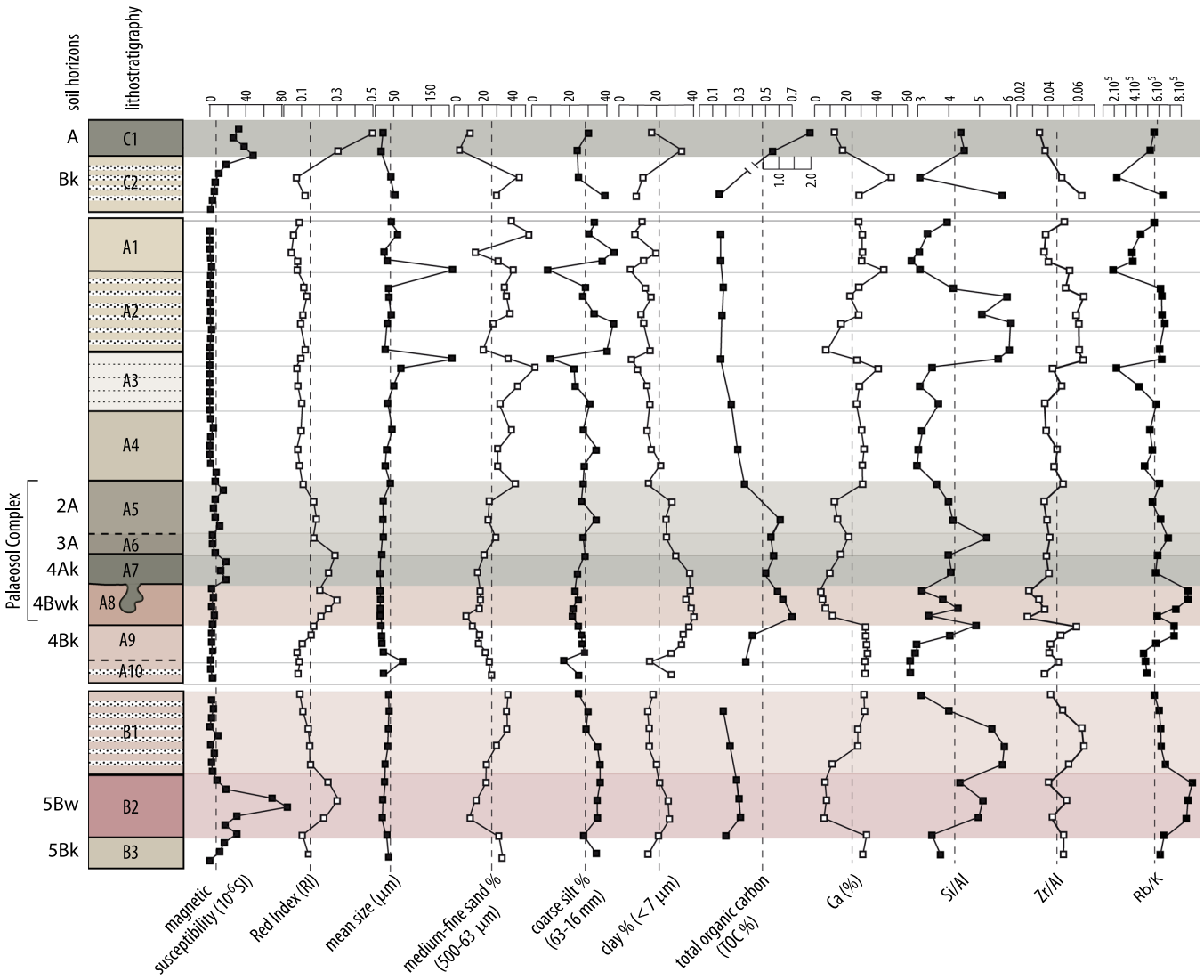

Figure 10. Evolution of magnetic susceptibility, Red Index, grain size, total organic carbon and chemical ratios along the stratigraphy. [Color figure can be viewed at wileyonlinelibrary.com]

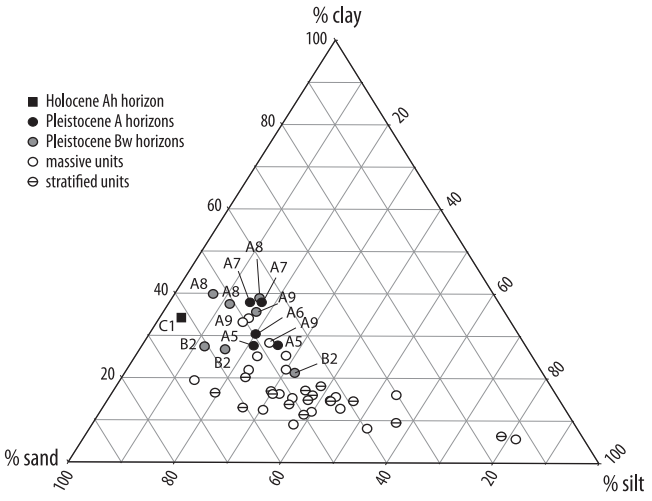

Figure 11. Grain size of the lithostratigraphic units in a sand-silt-clay diagram.

across northwestern Europe (Welter-Schultes, 2012). The snail *H. limbata* has similar ecological requirements but it is more common in forested habitats. Its modern range is less extended, centred on the Atlantic side of Europe (northwestern Spain, western France and the southwestern UK) (Welter-Schultes, 2012). In France, Quaternary occurrences of *H. limbata* and *Cepaea* are restricted to interglacial deposits (Limondin-Lozouet and Preece, 2014). These two taxa are representative of temperate climatic phases.

Luminescence dating

The results of OSL measurements are given in Tables 1,2 and 3. Both the average dose model (ADM, Guérin et al., 2017) and the central age model (CAM, Galbraith et al., 1999) were used. The results are indistinguishable, within uncertainties. The Kernel plots of the D_e distributions are presented in Supplementary Information Fig. S1. The distributions of equivalent dose values did not reveal any issues with poor bleaching or grain population mixing, even though this may be the result of an averaging effect due to the large number of grains measured together. According to Guérin et al. (2017), the ADM doses should be more accurate than CAM doses for determining burial ages; hence, we used the former dataset to calculate OSL ages. The radioelement content and external dose rates measured *in situ*, as well as the total dose rates, are presented in Table 2.

The OSL ages of the Verteuil samples are shown in Table 3 and Fig. 13. Within uncertainties (1σ), the chronological data obtained are consistent with the stratigraphic order. The deepest sample (BDX24864, unit B3) yielded an age of 146.9 ± 8.3 ka, which places its deposition during Marine Isotope Stage (MIS) 6.

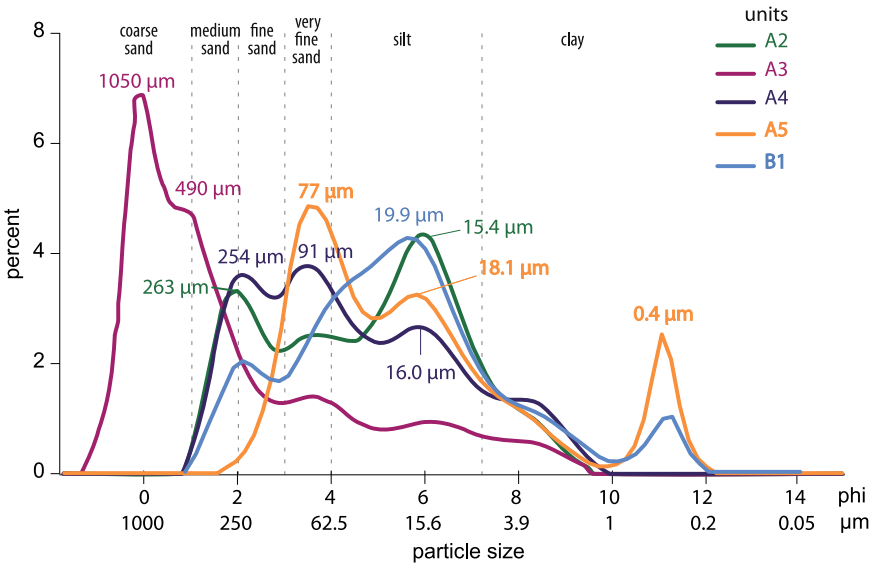

Figure 12. Grain-size curves of samples from units B1, A2 (stratified deposits), A3 (bedded sand), A4 (massive deposits) and A5 (2A horizon). [Color figure can be viewed at wileyonlinelibrary.com]

Table 1. Results of the D_e measurements. N: number of measured aliquots; n: number of aliquots that passed all tests (recycling and recuperation tests); D_e: equivalent dose; σ_d: intrinsic dispersion; OD: overdispersion.

			Average dose model		Central age model	
Lab. Ref.	N	n	D_e (Gy)	σ_d	D_e (Gy)	OD (%)
BDX24958	40	20	54.66 ± 0.63	0.05 ± 0.01	54.60 ± 0.63	5.01 ± 0.85
BDX24959	40	20	54.67 ± 0.61	0.05 ± 0.01	54.61 ± 0.63	5.00 ± 0.84
BDX24960	20	20	40.13 ± 0.35	0.04 ± 0.01	40.10 ± 0.35	3.80 ± 0.65
BDX24961	20	16	81.69 ± 1.19	0.06 ± 0.01	81.56 ± 1.23	5.92 ± 1.09
BDX24962	40	24	117.22 ± 1.24	0.04 ± 0.01	117.11 ± 1.20	4.59 ± 0.80
BDX24963	40	14	76.11 ± 1.17	0.06 ± 0.02	75.39 ± 0.85	3.96 ± 0.85
BDX24964	20	17	169.49 ± 3.43	0.08 ± 0.02	168.76 ± 3.74	8.75 ± 1.63

Table 2. Results of the determinations of annual dose rates.

Sample	K (%)	σ	U (226Ra, ppm)	σ	Th (ppm)	σ	*In situ* gamma dose rate (LaBr)	σ	Total dose rate (Gy.ka^{-1})	σ
BDX24958	0.44	0.01	1.69	0.03	3.11	0.05	327.84	6.51	1.17	0.04
BDX24959	0.56	0.01	1.93	0.03	3.79	0.05	253.11	5.03	1.22	0.05
BDX24960	0.32	0.01	1.74	0.02	2.71	0.04	168.82	3.36	0.91	0.04
BDX24961	0.78	0.02	2.57	0.03	6.94	0.07	284.06	5.64	1.57	0.07
BDX24962	0.91	0.02	3.07	0.04	8.94	0.09	670.58	13.31	2.12	0.09
BDX24963	0.37	0.01	1.66	0.02	3.03	0.04	146.77	2.92	0.88	0.04
BDX24964	0.48	0.01	1.68	0.02	3.90	0.05	179.60	3.57	0.99	0.04

Table 3. Results of OSL measurements of Verteuil samples; ages based on average dose model D_e measurements.

	Average dose model	
Lab. Ref.	Age (Gy)	σ
BDX24958	39.5	2.0
BDX24959	40.4	2.1
BDX24960	39.9	2.1
BDX24961	45.7	2.5
BDX24962	48.5	2.5
BDX24963	80.2	4.4
BDX24964	146.9	8.3

Unit A9 yielded an age of 80.2 ± 4.4 ka, i.e. MIS 5a or MIS 4. Therefore, Palaeosol 5Bw (unit B2) can be assigned to the Last Interglacial/Weichselian Early Glacial (MIS 5). The top of the palaeosol complex (units A5–A6) has an age between *ca.* 43 and 51 ka at the 68% confidence level (BDX24962: 48.5 ± 2.5 ka; BDX26961: 45.7 ± 2.5 ka), contemporary with the middle part of MIS 3 (i.e. GI-14a to GI-11; Rasmussen et al., 2014). The 4Ak horizon (unit A7) associated with burrows and the development of the underlying 4Bwk horizon (unit A8) could therefore be correlated with the beginning of MIS 3 (GI-16 to GI-14).

The ages of the top three samples in the sequence (BDX24958, BDX24959 and BDX24960) are indistinguishable and centred around 40 ka. MIS 2 (~27–15 ka) is poorly recorded and represents less than 1 m of deposits.

Discussion

Facies interpretation

Stratified deposits (units C2, A2, A10–B1)

Various processes have been proposed to explain the stratification of slope deposits (see review in Van Steijn et al., 1995,

2002). In the 1990s, Francou (1990) and Bertran et al. (1992, 1995) showed that stacking of stone-banked solifluction lobes best explained the characteristics of the Verteuil deposits. These processes, illustrated in Fig. 14, schematically involve: (1) upslope production of debris by frost wedging of limestone outcrops; (2) downslope redistribution of debris by solifluction, including frost-creep caused by freeze–thaw cycles (formation of ice needles in the subsurface and ice lenses at greater depths) and slow flow during ice thaw (gelifluction) (Harris et al., 2000). Localised shallow mudflows promoted by snowmelt can also contribute to movement (Matsuoka, 2010). As indicated above, rockfall plays only a very marginal role in the absence of a rock wall. Generalised solifluction over the slope results in large lobes or sheets that follow one another downhill and overlap as they progress. Each lobe/sheet comprises a surface pavement with a reverse grading generated by frost heave, washing during snowmelt and kinetic sieving, overlying a diamictic layer in which ice segregation takes place. At the base, a matrix-poor coarse-grained layer with a normal grading develops following the burial of the front stones. This dynamic accounts for the preferred slope–parallel clast orientation (Nelson, 1982; Bertran et al., 1997), clast imbrication, presence of recumbent folds in the matrix-rich levels, superposition of diamictic layers (central part of a lobe/sheet) and matrix-poor coarse-grained layers (buried pavements and stone fronts). We refer to the articles mentioned above for more detail. At the microscopic scale, evidence of eluviation and segregation ice lenses (silt caps, washed sands) is also consistent with such sedimentary dynamics (Harris and Ellis, 1980; Van Vliet-Lanoë, 2010). In units B1–A10, the reddish colour comes from the admixture of rubified matrix reworked from an older Bw horizon (unit B2).

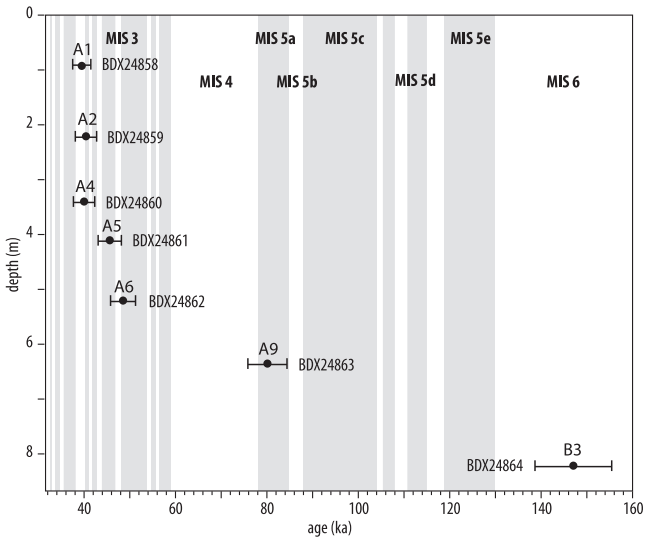

Figure 13. OSL ages as a function of sample depth. Interstadial boundaries are from Rasmussen et al. (2014). Lithostratigraphic units are shown above the ages. Grey bands indicate interglacial and interstadial periods.

At Verteuil, these processes most likely took place in a periglacial environment subject to frequent annual freeze–thaw cycles and sparse vegetation cover. In the region, similar processes are currently found in the Pyrenees above 2600–2800 m depending on the exposure (Feuillet, 2010) (Fig. 15). The grain-size mode in silts, associated with an increase in silicate minerals and especially zircon, strongly suggests that loess inputs contributed to sedimentation. As no loess deposits were observed on the plateau, the silts are assumed to reflect fresh dust accumulation, consistent with a periglacial context. The relatively fine mode of the particles (14–18 μm) indicates input from distant sources.

Massive diamictic and crudely stratified deposits (units A1, A4, A9, B3)

The massive diamictic deposits share some of the characteristics of stratified deposits, including preferred clast orientation, evidence of eluviation and segregation ice lenses, which suggest that solifluction was involved in their deposition. The high carbonate content, low Rb/K ratio and magnetic susceptibility values indicate a depositional setting unfavourable for weathering. The massive nature of the deposits makes it impossible to determine whether emplacement occurred during a single event (or a small number of significant events) or whether it resulted from progressive accretion. Comparison with present-day cold milieus suggests that several processes may have contributed to sedimentation. Depending on the context, the emplacement of diamictic layers may result from infrequent events of debris accumulation involving a large volume, such as debris flows caused by rainstorms, whereas processes related to freeze–thaw cycles occur seasonally (van Steijn et al., 1995). In this case, although it is not the main factor causing accumulation, solifluction modifies the internal structure of the sediments and leaves diagnostic features. In other cases, solifluction alone may generate thick diamictic layers in the absence of lobes (gradual accretion) or in a context where the formation of surface stone pavements is inhibited, particularly where a herbaceous cover develops (e.g. Matthews et al., 1986; Elliott and Worsley, 1999; Ballantyne, 2013). Modern analogues are shown in Fig. 15. In the Pyrenees, 'turf-banked' solifluction is well represented between 2200 and 2600 m. Finally, post-depositional homogenisation of the deposits, mainly by bioturbation, may also be at the origin of massive deposits.

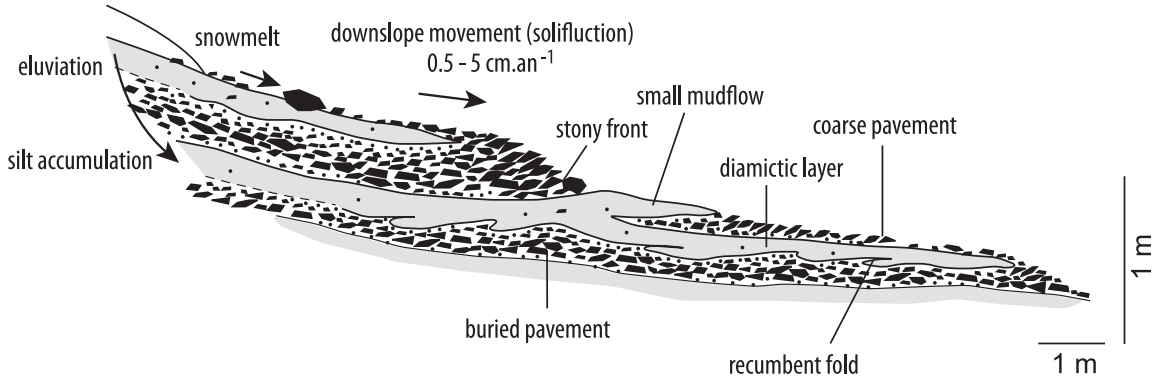

Figure 14. Schematic cross-section of a stone-banked solifluction lobe and associated processes, modified from Bertran et al. (1995).

Figure 15. Possible modern equivalents of the sedimentary processes recorded at Verteuil. A–stone-banked solifluction lobe, Central Pyrenees, 2760 m; B–section in a stone-banked solifluction lobe, same location; C–turf-banked solifluction lobes, Central Pyrenees, 2300 m; D–section in a turf-banked solifluction lobe, same location, note the buried A horizon below the diamictic layer; E–section in massive polygenic deposits (debris flows, solifluction, rock fall), Central Pyrenees, 2760 m. [Color figure can be viewed at wileyonlinelibrary.com]

This process may account for the presence of massive units under palaeosols (horizons 4Bwk and 5Bw).

Bedded sand and small gravel

Unit A3 corresponds to bedded calcareous sand and fine gravel intercalated between diamictic deposits. This level can be correlated laterally with a gully visible in frontal section (Fig. 7E). It may therefore represent a small colluvial fan formed at the outlet of a gully. Evidence of segregation ice lenses suggests that the blurred bed boundaries are related to downslope stretching of the deposits by frost-creep. Runoff is a ubiquitous process in contexts with sparse vegetation and it is difficult to determine whether these deposits resulted from a random event or were controlled by climate change.

Soil and palaeosols

The Holocene soil is a simple profile (Ah/Bk) typical of regional leptosols (IUSS Working Group World Reference Base, 2015) developed on limestone bedrock. These soils, largely influenced by agricultural practices, are characterised

by incomplete decalcification and a high content of organic matter stabilised by Ca^{2+} ions. Various palaeosols have been identified in the sequence. The palaeosol complex implies progressive soil accretion (cumulic soil) and/or a succession of sedimentation and soil formation phases. Fluctuations in Ca content, TOC and Rb/K ratio suggest that the latter hypothesis should be favoured here. Three horizons were thus distinguished (2A, 3A, 4Ahk). According to OSL ages, they reflect the succession of interstadials and stadials (Dansgaard-Oeschger cycles) typical of MIS 3. The 4Ahk horizon (unit A7), which shows secondary carbonate precipitation, overlies a slightly rubified cambic horizon (4Bwk). The 4Ahk/4Bwk profile can be interpreted as a cambisol contemporary with the long interstadials of early MIS 3, which involved stronger weathering and differentiation than for the Holocene soil. The 5Bw horizon, OSL-dated to MIS 5, is a rubified cambic horizon, with sharp lower and upper boundaries suggesting that it has been reworked on the slope. Thin-section observation shows that it had a complex history, including the formation of a slightly hydromorphic (Fe-Mn concretions) rubified clayey horizon, reworking on the slope (clay caps), followed by bioturbation.

Slope evolution

The deposits form a prism in the concavity of a meander of the Charente River (Fig. 3). Several generations of clastic units, each separated by an unconformity, can be distinguished. The unconformities result from erosion associated with a shift of the main depositional area. The oldest generation (unit B3) has a relatively strong dip (~14°) and has been dated to MIS 6. The MIS 5 soil is truncated and absent in the northern part of the quarry. The second generation of clastic deposits (units A9, A10 and B1), dipping about 11°, can be assigned to late MIS 5 and/or MIS 4. These deposits are stained reddish brown by the reworked MIS 5 soil material. A prominent unconformity separates the 4Ahk/4Bwk palaeosol (units A7–A8) formed on these deposits from the upper units (C1–A6), which dip 8–9°. Overall, the progressive lowering of the dip from the base to the top of the sequence reflects the growth of the debris mantle. As mentioned above, MIS 2 is poorly recorded and represents only about 1 m of deposits, possibly because of the reduction of the slope gradient and the accommodation space. Holocene (human-induced) erosion of the top deposits may also have played a role.

The lack of a direct link with the section described by Bertran et al. (1992), located in a former quarry about 110 m to the south, and of numerical dating in that section, makes correlation with the new section described here difficult. The most remarkable points that emerge from the comparison of the sequences are: (1) the significantly greater thickness of the upper unit of stratified deposits (beds 1 to 38, 'log A'; Bertran et al., 1992) in the old quarry, which reaches 5 m as opposed to less than 2 m (units C2–A2) in the new quarry; and (2) the greater dip of the layers, about 12–16° versus 9–11°. No dark brown humic horizon associated with burrows comparable to unit A7 was reported in the old section. The poorly stratified deposits described as a brown to reddish brown 'earthy grèze' at the base of the old sequence may be an equivalent of units A5–A6 in the new section. This hypothesis implies that the erosional surface that truncates unit A7 dips to the south and joins the base of the old section. The erosional surface would correspond to a small valley incised into the slope deposits during MIS 3, in which the formerly described stratified deposits accumulated over a great thickness. The old section would thus represent a thicker record of late MIS 3 and MIS 2.

Finally, the Verteuil sequence shows successive bodies of slope deposits, ranging in age from the Penultimate Glacial (MIS 6) to the present. This sequence includes major erosional phases, which seem to occur during or shortly after temperate climatic phases (Last Interglacial, early MIS 3). It is possible, but difficult to demonstrate from the available sections, that the incision phases were triggered by the erosion of the slope foot by the Charente River. Depending on the position in relation to the axis of the valleys, the record is of varying thickness. Overall, the cumulative thickness of sediment is considerable and reaches 12 m in total, i.e. about 7 m for the Last Glacial. This implies rapid debris production by frost wedging of the limestone and efficient processes of downslope debris transport in a periglacial context.

Comparison with other regional sequences of slope deposits

Stratified deposits

The chronological data obtained at Verteuil show that the stratified units C2–A2 attributed to stone-banked solifluction are younger than *ca.* 40 ka, i.e. they were deposited during late MIS 3 and MIS 2. The limited record of MIS 2 in this section does not allow for further detail. Unit B1 is located within the Weichselian Early Glacial and may correspond to the MIS 5d or MIS 5b cold phases. Some sections of southwest France in an archaeological context also show similar stratified deposits. At Les Peyrugues (Bertran, 2005), the ^{14}C ages obtained from archaeological material (charcoal, bone) range from *ca.* 26 to 21 ka cal BP. At La Ferrassie (Bertran et al., 2008), the single ^{14}C date available for this facies places its emplacement around 24 ka cal BP. At Abri Pataud (Lenoble and Agsous, 2012), the stratified units are dated to between *ca.* 28 and 25 ka cal BP. Altogether, the chronological dataset indicates that stratified deposits developed during the coldest periods of the glacial, particularly during the 28–21 ka interval (first part of MIS 2), which is consistent with the hypothesis of periglacial depositional processes. Some MIS 3 (around 40 ka) and MIS 5 stadials were also favourable for these processes.

Palaeosols

Other sections of slope deposits located in Charente on Jurassic limestone show palaeosols that were mentioned by Dewolf and Guillien (1962), Guillien (1965), Ducloux et al. (1970), Ducloux (1972), Ozouf (1983) and Ozouf et al. (1995) and were attributed to interglacial or interstadial periods. However, the palaeosols have not been precisely described and analysed, except by Ducloux (1972) and Ducloux et al. (1970). Guillien and Puisségur (1969) also reported on the malacological fauna found in palaeosols, which was either typical of temperate forests or colder steppe-like environments. In the Vars-Beaumont and Echoisy quarries (Fig. 1), Ducloux et al. (1970) described rubified palaeosols (2.5YR to 5YR), characterised by incomplete decalcification, clay formation and well-crystallised goethite. These palaeosols, related to the Eemian interglacial, are considered close to Mediterranean red soils (*cf.* chromic cambisols; IUSS Working Group World Reference Base, 2015), developed under relatively humid temperate conditions with a marked dry season. In the Sonneville quarry, a palaeosol attributed to a Weichselian interstadial consists of a brown horizon (10YR) that is slightly decalcified, richer in organic matter and iron oxides than the underlying deposits, and marked by the development of vermiculite, which derives from the transformation of smectite inherited from the parent limestone. It would have formed in a well-drained temperate or cold context. At Echoisy, Guillien (1965) reported a red palaeosol attributed to the Eemian

interglacial with burrows of marmots or ground squirrels. It is associated with an abundant molluscan fauna composed solely of individuals of the species *Cepaea hortensis* (J.J. Puisségur, in Guillien, 1965).

As the quarries mentioned above have largely evolved due to their exploitation or have been filled in after their abandonment, the palaeosols described have for the most part not been found again. At Sonneville, a rubified palaeosol, probably largely reworked, is still visible. As indicated by Ozouf et al. (1995), it is truncated by a major unconformity separating two generations of slope deposits. The high clay content and strong rubefaction are similar to those of the 5Bw horizon of Verteuil. It could therefore be contemporary with the Eemian interglacial, in agreement with Ozouf et al. (1995).

Partially or totally decalcified levels with varying organic matter content have also been described in the context of cave porches and rock shelters. There is a debate in the literature about the anthropogenic or natural origin of the organic matter and, consequently, about the significance of these levels (e.g. Goldberg and Sherwood, 2006; Pirson et al., 2006; Bertran et al., 2008; Ajas et al., 2013; Goldberg et al., 2018). Different arguments have been proposed by Bertran et al. (2008) and Ajas et al. (2013) in favour of their interpretation as palaeosols modified to varying degrees by anthropogenic activity. The palaeosols can be classified mostly among leptosols and cambisols according to their development. These arguments are as follows:

(1) Weathering and decalcification cannot be the result of anthropogenic activity but reflect the percolation of water desaturated with respect to calcite over a long period. Preserved root concretions indicate that part of the dissolved carbonates from the upper soil horizons have precipitated at depth in association with biological activity (Bertran et al., 2008). The ^{14}C and thermoluminescence ages obtained on the sequences also argue in favour of decalcification that is even more pronounced as the interruption of sedimentation was long (Ajas et al., 2013). At many cave sites, the accumulation of phosphate-rich excrements by fauna (carnivores, bats) led to acidification of percolating water and almost complete decalcification of sediments.
(2) The accumulation of organic molecules in sufficient amounts to compensate for losses by mineralisation and to allow the formation of humic A horizons implies renewed and important inputs of fresh organic matter to the soil and mixing with the mineral material by biological activity. Such inputs are not compatible with brief Palaeolithic occupations. The organic molecules (n-alkanes, alcohols and fatty acids), adsorbed on clays, were mainly derived from higher plants, bacteria and fungi (Bertran et al., 2008), as in Holocene soils on limestone. By contrast, molecules of animal origin are rare. At Combe Saunière (Ajas et al., 2013), however, a dark horizon rich in long-chained alkylbenzenes and polyaromatic hydrocarbons produced by combustion testifies to an origin linked to human activities at this site.
(3) The sharp horizon boundaries and the near absence of visible bioturbation at the microscopic scale are related to later deformation of the palaeosols by cryogenic processes on the slope. Microscopic structures related to ice segregation and washing (platy structures, silty caps on clasts) are common (Bertran et al., 2008).

According to the above-mentioned arguments, humic horizons (modified to varying degrees by anthropogenic activity) would have developed mainly during MIS 3 ('black' horizons typical of the Aurignacian (~41–35 ka), e.g. Bertran et al., 2008; Ajas et al., 2013), but also at the end of MIS 5 (Guérin et al., 2012b; Goldberg et al, 2018), while rubified more strongly decalcified Bw horizons would have formed during the beginning of MIS 3 (associated with Late Mousterian) and MIS 5 (Ajas et al., 2013; Goldberg et al., 2018). The presence of similar palaeosols in an open-air context at Verteuil with no evidence of Palaeolithic occupation suggests that they are representative of the regional evolution of slopes on limestone and reflect global climate variations.

Conclusion

The study of the slope deposit exposed in the Verteuil quarry, which includes a succession of clastic levels and palaeosols over a thickness of nearly 12 m, makes it possible to establish for the first time a detailed chronostratigraphy for this type of Quaternary deposit in southwest France. The main clastic units separated by major unconformities were dated to MIS 6, MIS 5–4 and MIS 3–2, respectively. Thick stratified deposits, consisting of alternating diamictic and openwork clastic beds and attributed to stone-banked solifluction lobes/sheets, developed mainly after *ca.* 40 ka, i.e. during late MIS 3 and MIS 2. The MIS 3 palaeosol complex consists of at least two humic A horizons associated with secondary carbonate accumulations (Bk horizons), overlying a more complex Ahk/Bwk/Bk profile related to a chromic cambisol. The latter was dated to the first half of MIS 3 (earlier than *ca.* 48 ka). At the regional scale, this palaeosol complex has an equivalent in caves and rock shelters in the humic horizons typical of the Early Upper Palaeolithic and in the underlying rubified horizons associated with Late Mousterian. The Eemian–Early Glacial is marked by a thick rubified horizon (Bw) reworked on the slope.

In the studied section, the MIS 2 deposits are of limited thickness and develop more largely to the south, where they have been described previously (Bertran et al., 1992, 1994). The former quarry has been backfilled, but there are still active quarries a few hundred metres to the south. Study and dating of the deposits visible in the latter should provide a more detailed chronostratigraphy for the late Pleistocene.

Acknowledgements. We thank the owner of the quarry, M. de La Rochefoucauld, for allowing us to sample the section, as well as J.P. Faivre (PACEA, CNRS-University of Bordeaux) for financing OSL dating as part of the NATCH project (Région Nouvelle-Aquitaine) (2016 – 1R40204 – 00007349 – 00007350). This work was carried out within the framework of J. Puyrigaud's Masters thesis supervised by P. Bertran.

Data availability statement

The data that support the findings of this study are available from the corresponding author upon reasonable request.

Supporting information

Additional supporting information can be found in the online version of this article.

Figure S1: Kernel plots of the D_e distributions

Abbreviations. MIS, Marine Isotope Stage; OSL, Optically Stimulated Luminescence; IGN, Institut Géographique National; LiDAR, Light Detection And Ranging; RI, Red Index; TOC, Total organic Carbon; SAR, Single-Aliquote Regeneration; pLM-OSL, Pseudo-Linearly Modulated Optically Stimulated Luminescence; ADM, Average Dose Model; CAM, Central Age Model.

References

Aitken, M.J. & Xie, J. (1990) Moisture correction for annual gamma dose. *Ancient TL*, 8(2), 6–9.

Ajas, A., Bertran, P., Lemée, L. & Queffelec, A. (2013) Stratigraphy and palaeopedology of the Palaeolithic cave site of Combe-Saunière, southwest France. *Geoarchaeology, an International Journal*, 128, 432–449.

Aubry, M.P. & Lautridou, J.P. (1974) Relations entre propriétés physiques, gélivité et caractères microstructuraux dans divers types de roches: craies, calcaires crayeux, calcaire sublithographique et silex. *Bulletin du Centre de Géomorphologie du CNRS de Caen*, 19, 7–16.

Ballantyne, C. (2013) A 35-year record of solifluction in a maritime periglacial environment. *Permafrost and Periglacial Processes*, 24, 56–66.

Barron, V. & Torrent, J. (1986) Use of the Kubelka-Munk theory to study the influence of iron oxides on soil colour. *Journal of Soil Science*, 37(4), 499–510.

Bertran, P. (2005) Stratigraphie du site des Peyrugues (Lot), une coupe de référence pour le dernier Pléniglaciaire en Aquitaine. *Quaternaire*, 16(1), 25–44.

Bertran, P., Caner, L., Langohr, R., Lemée, L. & d'Errico, F. (2008) Continental palaeoenvironments during MIS 2 and 3 in south-western France: the La Ferrassie rockshelter record. *Quaternary Science Reviews*, 27, 2048–2063.

Bertran, P., Coutard, J.P., Francou, B., Ozouf, J.C. & Texier, J.P. (1992) Nouvelles données sur l'origine du litage des grèzes. Implications paléoclimatiques. *Géographie Physique et Quaternaire*, 46(1), 97–112.

Bertran, P., Coutard, J.P., Francou, B., Ozouf, J.C. & Texier, J.P. (1994) New data on grèzes litées bedding and their palaeoclimatic implications. In: Evans, D.J.A., (Ed.) *Cold Climate Landforms*. Chichester: Wiley. pp. 437–454.

Bertran, P., Francou, B. & Texier, J.P. (1995) Stratified slope deposits: the stone-banked sheets and lobes model. In: Slaymaker, O., (ed.) *Steepland Geomorphology*. Wiley. pp. 147–169.

Bertran, P., Hétu, B., Texier, J.P. & Van Steijn, H. (1997) Fabric characteristics of slope deposits. *Sedimentology*, 44, 1–16.

Bos, A.J. & Wallinga, J. (2012) How to visualize quartz OSL signal components. *Radiation Measurements*, 47(9), 752–758.

Bosq, M., Bertran, P., Degeai, S.P., Queffelec, A. & Moine, O. (2020) Geochemical signature of sources, recycling and weathering in the Last Glacial loess from the Rhône Valley (southeast France) and comparison with other European regions. *Aeolian Research*, 42, 100561.

Buggle, B., Glaser, B., Hambach, U., Gerasimenko, N. & Marković, S. (2011) An evaluation of geochemical weathering indices in loess–paleosol studies. *Quaternary International*, 240, 12–21.

Bullock, P., Fédoroff, N., Jongerius, A., Stoops, G. & Tursina, T. (1985) *Handbook for soil thin section description*. Wolverhampton: Waine Research Publishers. p. 152.

Bulur, E. (2000) A simple transformation for converting CW-OSL curves to LM-OSL curves. *Radiation Measurements*, 32(2), 141–145.

Cariou, E. & Gabilly, J. (1973) *Notice explicative de la feuille de Ruffec à 1/50 000*. Orléans: Bureau des Recherches Géologiques et Minières. p. 11.

Dewolf, Y. & Guillien, Y. (1962) Les paléosols des grèzes françaises. *Comptes Rendus Sommaires de la Société Géologique de France*, 3, 90–92.

Ducloux, J. (1972) Etude paléopédologique des grèzes périglaciaires de Sonneville (Charente). *Bulletin de l'Association Française pour l'Etude du Quaternaire*, 9(2), 125–133.

Ducloux, J., Dupuis, J., Guillien, Y. & Puisségur, J.J. (1970) Paléosols interglaciaires des grèzes de Beaumont et d'Échoisy (Charente). *Bulletin de l'Association Française pour l'Etude du Quaternaire*, 7(2), 121–133.

Elliott, G. & Worsley, P. (1999) The sedimentology, stratigraphy and 14C dating of a turf-banked solifluction lobe: evidence for Holocene slope instability at Okstindan, northern Norway. *Journal of Quaternary Science*, 14(2), 175–188.

Ellwood, B.B., Harrold, F.B., Benoist, S.L., Thacker, P., Otte, M., Bonjean, D. et al. (2004) Magnetic susceptibility applied as an age–depth–climate relative dating technique using sediments from Scladina Cave, a Late Pleistocene cave site in Belgium. *Journal of Archaeological Science*, 31(3), 283–293.

Feuillet, T. 2010. Les formes périglaciaires dans les Pyrénées centrales françaises: analyse spatiale, chronologique et valorisation. PhD thesis, University of Nantes, 405

Francou, B. (1990) Stratification mechanisms in slope deposits in high subequatorial mountains. *Permafrost and Periglacial Processes*, 1, 249–263.

Galbraith, R.F., Roberts, R.G., Laslett, G.M., Yoshida, H. & Olley, J.M. (1999) Optical dating of single and multiple grains of quartz from Jinmium rock shelter, northern Australia: Part I, Experimental design and statistical models. *Archaeometry*, 41(2), 339–364.

Gallet, S., Jahn, B., Van Vliet-Lanoë, B., Dia, A. & Rossello, E. (1998) Loess geochemistry and its implications for particle origin and composition of the upper continental crust. *Earth and Planetary Science Letters*, 156, 157–172.

Goldberg, P., McPherron, S.P., Dibble, H.L. & Sandgathe, D. (2018) Stratigraphy, deposits, and site Formation. In: Dibble, H.L. et al., (Eds.) *The Middle Paleolithic Site of Pech de l'Azé IV*. Cave and Karst Systems of the World, Springer In: https://doi.org/10.1007/978-3-319-57524-7_2

Goldberg, P. & Sherwood, S.C. (2006) Deciphering human prehistory through the geoarchaeological study of cave sediments. *Evolutionary Anthropology*, 15, 20–36.

Guérin, G., Christophe, C., Philippe, A., Murray, A.S., Thomsen, K.J., Tribolo, C. et al. (2017) Absorbed dose, equivalent dose, measured dose rates, and implications for OSL age estimates: Introducing the Average Dose Model. *Quaternary Geochronology*, 41, 163–173.

Guérin, G., Discamps, E., Lahaye, C., Mercier, N., Guibert, P., Turq, A. et al. (2012b) Multi-method (TL and OSL), multi-material (quartz and flint) dating of the Mousterian site of Roc de Marsal (Dordogne, France): correlating Neanderthal occupations with the climatic variability of MIS 5-3. *Journal of Archaeological Science*, 39, 3071–3084.

Guérin, G. & Mercier, N. (2011) Determining gamma dose rates by field gamma spectroscopy in sedimentary media: results of Monte Carlo simulations. *Radiation Measurements*, 46(2), 190–195.

Guérin, G., Mercier, N. & Adamiec, G. (2011) Dose-rate conversion factors: update. *Ancient TL*, 29(1), 5–8.

Guérin, G., Mercier, N., Nathan, R., Adamiec, G. & Lefrais, Y. (2012a) On the use of the infinite matrix assumption and associated concepts: a critical review. *Radiation Measurements*, 47(9), 778–785.

Guibert, P. & Schvoerer, M. (1991) TL dating: low background gamma spectrometry as a tool for the determination of the annual dose. *Nuclear Tracks and Radiation Measurements*, 18, 231–238.

Guillen, Y. (1954) Le litage des grèzes. *Comptes Rendus de l'Académie des Sciences de Paris*, 238, 2250–2251.

Guillen, Y. (1964) Les grèzes comme dépôt cyclothémique. *Zeitschrift für Geomorphologie, Suppl.-Band*, 5, 53–58.

Guillien, Y. (1951) Les grèzes litées de Charente. *Revue Géographique des Pyrénées et du Sud-Ouest*, 22, 153–162.

Guillien, Y. (1965) Dépôts de pente, terrasses, remblaiements holocènes entre Angoulême et Mansle. *Bulletin de l'Association Française pour l'Etude du Quaternaire*, 2(3), 251–256.

Guillien, Y. & Puisségur, J.J. (1969) Géomorphologie et malacologie de quelques dépôts de pente charentais. *Comptes rendus hebdomadaires des séances de l'Académie des sciences de Paris, Série D, Sciences naturelles*, 268, 24–27.

Harris, C. & Ellis, S. (1980) Micromorphology of soils in soliflucted materials, Okstindan, Northern Norway. *Geoderma*, 23, 11–29.

Harris, C., Murton, J. & Davies, M.C.R. (2000) Soft sediment deformation during thawing of ice-rich frozen soils: results of scaled centrifuge modelling experiments. *Sedimentology*, 47, 687–700.

IUSS Working Group World Reference Base. (2015) *World reference base for soil resources 2014, update 2015. International soil classification system for naming soils and creating legends for soil maps*. RomeWorld soil resources reports 106: Food and Agriculture Organization of the United Nations.

Lautridou, J.P. & Leneuf, N. (1974) Microstructure et gélivité des calcaires lithographiques. *Bulletin du Centre de Géomorphologie du CNRS de Caen*, 19, 17–23.

Lebrun, B., Frerebeau, N., Paradol, G., Guérin, G., Mercier, N., Tribolo, C. et al. (2020) Gamma: An R Package for Dose Rate Estimation from In-Situ Gamma-Ray Spectrometry Measurements. *Ancient TL*, 18, 1–5.

Lenoble, A. & Agsous, S. (2012) Abri Pataud—Sédimentogenèse, paléopédologie, chronologie des dépôts. In: Bertran, P. & Lenoble, A., (Eds.) *Guidebook of the 2012 AFEQ-ASF field excursion*. Association Française pour l'Etude du Quaternaire. pp. 45–58.

Limondin-Lozouet, N. & Preece, R.C. (2014) Quaternary perspectives on the diversity of land snail assemblages from NW Europe. *Journal of Molluscan Studies*, 80, 224–237.

Maher, B.A. & Thompson, R. (1991) Mineral magnetic record of the Chinese loess and paleosols. *Geology*, 19(1), 3.

Matsuoka, N. (2010) Solifluction and mudflow on a limestone periglacial slope in the Swiss Alps: 14 Years of Monitoring. *Permafrost and Periglacial Processes*, 21, 219–240.

Matthews, J.A., Harris, C. & Ballantyne, C. (1986) Studies on a gelifluction lobe, Jotunheimen, Norway: 14C chronology, stratigraphy, sedimentology and palaeoenvironment. *Geografiska Annaler*, 68A, 345–360.

Miallier, D., Guérin, G., Mercier, N., Pilleyre, T. & Sanzelle, S. (2009) The Clermont radiometric reference rocks: a convenient tool for dosimetric purposes. *Ancient TL*, 20, 37–43.

Mullins, C.E. (1977) Magnetic susceptibility of the soil and its significance in soil science. *Journal of Soil Science*, 28(2), 223–246.

Murray, A.S. & Wintle, A.G. (2000) Luminescence dating of quartz using an improved single-aliquot regenerative-dose protocol. *Radiation Measurements*, 32, 57–73.

Murray, A.S. & Wintle, A.G. (2003) The single aliquot regenerative dose protocol: potential for improvements in reliability. *Radiation Measurements*, 37, 377–381.

Nelson, F.E. (1982) A preliminary investigation of solifluction macrofabrics. *Catena*, 12, 23–33.

Nesbitt, H.W., Markovics, G. & Price, R.C. (1980) Chemical processes affecting alkalis and alkaline earths during continental weathering. *Geochimica et Cosmochimica Acta*, 44, 1659–1666.

Ozouf, J.C. 1983. Comparaison de gélifracts naturels de grèzes charentaises et de gélifracts fabriqués: étude expérimentale et traitement statistique, application des méthodes d'analyse des données. PhD thesis, University of Caen, 158 p.

Ozouf, J.C., Texier, J.P., Bertran, P. & Coutard, J.P. (1995) Quelques coupes caractéris-tiques dans les dépôts de versant d'Aquitaine septentrionale: faciès et interprétation dynamique. *Permafrost and Periglacial Processes*, 6, 89–101.

Pirson, S., Haesaerts, P., Court-Picon, M., Damblon, F., Toussaint, M., Debenham, M. et al. (2006) Belgian cave entrance and rock-shelter sequences as palaeoenvironmental recorders: The example of Walou cave. *Geologica Belgica*, 9/3(4), 275–286.

Ponomarenko, D. & Ponomarenko, E. (2019) Describing krotovinas: A contribution to methodology and interpretation. *Quaternary International*, 502, 238–245.

Rasmussen, S.O., Bigler, M., Blockley, S.P., Blunier, T., Buchard, S.L., Clausen, H.B. et al. (2014) A stratigraphic framework for abrupt climatic changes during the Last Glacial period based on three synchronized Greenland ice-core records: refining and extending the INTIMATE event stratigraphy. *Quaternary Science Reviews*, 106, 14–28.

Richter, D., Richter, A. & Dornich, K. (2015) Lexsyg smart—a luminescence detection system for dosimetry, material research and dating application. *Geochronometria*, 42(1), 202–206.

Royer, A., Montuire, S., Legendre, S., Discamps, E., Jeannet, M. & Lécuyer, C. (2016) Investigating the influence of climate changes on rodent communities at a regional-scale (MIS 1-3, southwestern France). *PLoS One*, 11(1), e0145600.

Sheldon, N.D. & Tabor, N.J. (2009) Quantitative paleoenvironmental and paleoclimatic reconstruction using paleosols. *Earth Science Reviews*, 95(1-2), 1–52.

Texier, J.P. 1986. Les dépôts de pente carbonatés du Périgord: caractéristiques, genèse, chronologie. In: *Especial Jean Roche-II*, Arqueologia (Porto) 13: 13-30.

Van Steijn, H., Bertran, P., Francou, B., Hétu, B. & Texier, J.P. (1995) Review of models for genetical interpretation of stratified slope deposits. *Permafrost and Periglacial Processes*, 6, 125–146.

Van Steijn, H., Boelhouwers, J., Harris, S. & Hétu, B. (2002) Recent research on the nature, origin and climatic relations of blocky and stratified slope deposits. *Progress in Physical Geography*, 26(4), 551–575.

Van Vliet-Lanoë, B. (2010) Frost action. In: Stoops, G., Marcelino, V. & Mees, F., (Eds.) *Interpretation of Micromorphological Features of Soils and Regoliths*. Amsterdam: Elsevier. pp. 81–108.

Viscarra Rossel, R.A., Minasny, B., Roudier, P. & McBratney, A.B. (2006) Colour space models for soil science. *Geoderma*, 133(3-4), 320–337.

Welter-Schultes, F.W. (2012) *European non-marine molluscs, a guide for species identification*. Göttingen: Planet Poster Editions.

Wintle, A.G. & Murray, A.S. (2006) A review of quartz optically stimulated luminescence characteristics and their relevance in single-aliquot regeneration dating protocols. *Radiation Measurements*, 41, 369–391.

Zimmerman, D.W. (1971) Thermoluminescent dating using fine grains from pottery. *Archaeometry*, 13(1), 29–52.